Quantum computation with electrons trapped on liquid Helium by using the centimeter-wave manipulating techniques

Yufen Li[1] · Suirong He[1] · Miao Zhang[2] · Lianfu Wei[1]

Abstract

Surface-state electrons floating on liquid Helium have been served as one of the great potential experimental platforms to implement quantum computation, wherein the qubits are usually encoded by either the lowest two levels of the vertical vibrations (i.e., Hydrogen-like atoms) or the electronic spins. Given the relevant operations require additional techniques, such as the corresponding millimeter-wave or magnetic field manipulations, here we investigate how to implement the scalable quantum computation with a trapped electron array by alternatively using the usual centimeter-wave manipulating techniques. This is because the eigenfrequency of the present qubit, encoded by the two lowest levels of the lateral vibration of the trapped electron, is limited in the centimeter-wave band. We show that, by biasing the electrodes properly and driving the coplanar waveguide transmission line resonator, the electrons can be individually trapped in a series of anharmonic potentials on liquid Helium. Therefore, the well-developed circuit quantum electrodynamics technique for the implementation of superconducting quantum computation can be conveniently utilized here in the present quantum computing platform (proposed firstly in Phys Rev Lett 105:040503, 2010, to implement the fundamental logic gates, typically such as the single-qubit rotations of the individually addressable trapped electrons, the switchable two-qubit

---

✉ Lianfu Wei
lfwei@swjtu.edu.cn

Yufen Li
yfli@my.swjtu.edu.cn

Suirong He
hesuirong@163.com

Miao Zhang
zhangmiao@swjtu.edu.cn

[1] Information Quantum Technology Laboratory, International Cooperation Research Center of China Communication and Sensor Networks for Modern Transportation, School of Information Science and Technology, Southwest Jiaotong University, Chengdu 610031, Sichuan, China

[2] School of Physics Science and Technology, Southwest Jiaotong University, Chengdu 610031, Sichuan, China

manipulations between the electrons trapped in the distant traps, and also the high-fidelity readouts of the target qubits. The feasibility of the proposal is also discussed by numerical simulations.

Keywords Electrons on liquid Helium · Lateral orbital states · Qubits · Addressable manipulations · Quantum computation

1 Introduction

The researches of practical quantum computation have been paid much attention in recent years [1]. In 2019, the so-called quantum supremacy has first been demonstrated with 53-bit programmable superconducting qubits, and thus, using the quantum processors to exponential speedup over its classical counterpart is desirably feasible [2]. In addition, a series of experimentally quantum information processors, typically, e.g., the linear optical Bose sampler [3], superconducting adiabatic quantum quenching [4], and the optical coherent Ising machines [5, 6], have also demonstrated the realistic possibility of the quantum computation. Indeed, a series of physical systems, typically such as the superconducting Josephson junction circuits [7], trapped ions [8–14], linear optical quantum systems [15, 16], and also the semiconductor quantum dot arrays [17, 18], have been demonstrated to implement the desired quantum computation.

In comparison, although either the Hydrogen-like atomic states [19] or the spin states [20] of electrons trapped on liquid Helium had been demonstrated to encode the qubits for the implementation of quantum computation, the desired universal quantum computation with such a system has not been implemented yet. Probably, this is due to certain realistic difficulties. For example, the millimeter-wave (MMW) pulse technique (rather than the usual centimeter-wave (CMW) one applied widely in the circuit quantum electrodynamics (QED) system) is required to implement the manipulations of the qubits encoded by the lowest two levels of the vertical vibration of the trapped electrons (i.e., the Hydrogen-like atom) [19]. However, given such a physical system possesses certain unique advantages, typically such as the particularly pure environment with significantly less noise [20, 21] and the relatively easy to be scalable by conveniently setting the electrodes at the bottom of Helium to generate the qubit array [22], quantum computation with the electrons trapped on liquid Helium is still desirable. In fact, benefiting from the significantly long coherent times of the Hydrogen-like atomic states and the electric spin states, various coherent quantum manipulations have been proposed theoretically, e.g., the realization of Jaynes–Cummings model [23, 24], image charge detection of Rydberg state [25, 26], spin state controls [27], and possible MMW photonic crystals with adjustable band gaps [28], have been proposed. Note that most of these manipulations are performed on the vertical-state qubits, generated by vibration of the electron along the direction which is perpendicular to the liquid Helium surface, and the MMW-pulse technique [29], instead of the well-developed CMW one, is required to be developed particularly.

Interestingly, Schuster et al. [22] demonstrated that the lateral motion of the electrons on liquid Helium can also be trapped by applying properly biased electrodes at the bottom of liquid Helium. Given the transition frequency of the qubits encoded
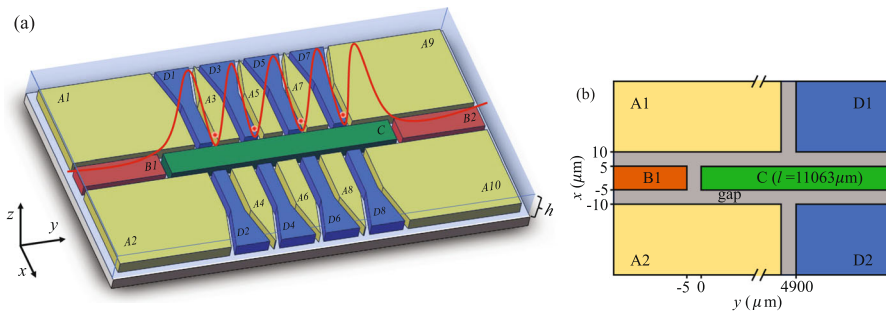
(a)

(b)

Fig. 1 A trapped electron array on liquid Helium generated by the DC-bias electrodes and an rf-driving CPW-TLR. **a** The designed chip, wherein A1–A10 are the grounds, B1 and B2 are the CPW feed lines separated by a CPW-TLR (C), and D1–D8 are the DC-biased electrodes used to confine the x-direction motions of the trapped electrons, and the surface of the chip is covered by a layer of liquid Helium with the thickness $h \sim 500$ nm [34]. Besides the trapped potentials generated by the voltage-biased electrodes, a standing wave along the y-direction is also excited by the CPW-TLR. Thus, a series of anharmonic potential wells are generated to trap a series of electrons on liquid Helium. **b** The parameters of a unit of the designed chip. The unit size is 12000 μm×100 μm, the thickness of the sapphire substrate is set as 400 μm, and the widths of the TLR and the gaps are set as 10 μm and 5 μm, respectively

by the lowest two levels of these orbital quantum states is in the usual CMW band, demonstrated firstly in Ref. [27], the circuit QED technique can be applied to implement the qubits manipulation by driving the quantized transmission line resonators placed at the bottom of liquid Helium [22]. Inspired by these pioneer works, in this paper we discuss the feasibility of using the lateral nonharmonic motion (rather than the vertical Hydrogen-like atoms) of the trapped electrons to implement quantum computation. We first designed the qubit array on liquid Helium. Then, we investigate the robustness of the present qubits and the feasibility of the quantum manipulations for scalable quantum computation both analytically and numerically.

The paper is organized as follows: In Sect. 2, we design a generic one-dimensional potential array to confine the electrons in a series of traps on liquid Helium. It is shown that the lowest two levels of the lateral anharmonic vibration of the electron in each trap can be utilized to encode the qubit, whose eigenfrequency is in the CMW band. In Sect. 3, by making use of a driven coplanar waveguide transmission line resonator (CPW-TLR) at the bottom of liquid Helium as the date bus, we demonstrate how to implement the addressable single-qubit operations and the switchable two-qubit logic gate operations between two arbitrarily selected distant qubits. The quantum non-demolition (QND) readout(s) of the qubit(s) in both frequency and time domains are simulated numerically in Sect. 4. We show also here that the pure and mixed states of the qubits could be distinguished effectively. Finally, the conclusion is given in Sect. 5.

2 The robustness of the qubit encoded by the lateral anharmonic vibration of the electron trapped on liquid Helium

Let us consider a planar chip schematically shown in Fig. 1, wherein a series of electrons are trapped individually on liquid Helium and thus generate a trapped electron

array. Floating electrons on liquid Helium had been demonstrated experimentally many years ago (see, e.g., [29]), as Helium is a noble gas that can be liquidated at a temperature below about 4.125 K. According to the Pauli exclusion principle, a potential barrier (about 1 eV [30]) prevents the electron from the liquid Helium. As a consequence, the electron can be floated on liquid Helium and its motion along the vertical direction generates a Hydrogen-like atom. In fact, electrons floating on liquid Helium have also served as one of the promising platforms to investigate various physical behaviors of two-dimensional electron gas [31, 32] and Wigner crystal [28, 33]. Experimentally, various interesting physical effects of the electrons trapped on liquid Helium have been widely investigated [34, 35]. Alternatively, to implement the desired quantum computation in CMW band, in the present work, we focus on the quantum manipulations of a series of single electrons trapped on liquid Helium. For the manipulability, the potentials for trapping the electrons can be generated by the voltage-biased electrodes at the bottom of liquid Helium and driven by coupling with the CPW-TLR.

2.1 Quantization of the lateral vibrations of the trapped electrons on liquid Helium

We design a chip shown in Fig. 1 for the scalable quantum computation with the electrons trapped in a series of potentials, generating a Pauli-like trap array. The dynamics a single trapped electron can be described by the Hamiltonian:

$$\hat{H}_{sys} = \hat{H}_r + \hat{H}_a + \hat{H}_I, \tag{1}$$

where $\hat{H}_r = \hbar\omega_r\hat{a}_r^\dagger\hat{a}_r$ describe the standing wave magnetic field in the CPW-TLR, $\hat{H}_a$ is for the lateral vibration of the trapped electron, and $\hat{H}_I = e\hat{d}\hat{E}_{rf}$ refers to the electric–dipole interaction between the electron and field in the resonator. Specifically, the Hamiltonian of the electron can be written as

$$\hat{H}_a = \frac{\hat{p}^2(z, x, y)}{2m} + U(z, x, y) = \hat{H}_z + \hat{H}_x + \hat{H}_y. \tag{2}$$

Here, the trap potential of the electron reads [19, 34]:

$$U(x, y, z) = -\frac{\Lambda e^2}{4\pi\varepsilon_0 z} + eE_{dc}\sqrt{(h+z)^2 + x^2 + y^2}, \tag{3}$$

where e is the electronic charge, h represents the thickness of liquid Helium, z is the vertical vibration of the trapped electron along the z-direction, and E_{dc} is obtained by the biased electrodes at the bottom of liquid Helium. Also, $\Lambda = (\varepsilon - 1)/[4(\varepsilon + 1)]$ with $\varepsilon = 1.06$ and ε_0 are the relative permittivity of liquid Helium and the vacuum permittivity, respectively. As $x, y, z \ll h$, the above potential can be effectively

approximated as

$$U \approx -\frac{\Lambda e^2}{4\pi \varepsilon_0 z} + \frac{e E_{dc} \left(8h^4 + 8h^3 z + 4h^2 x^2 - x^4 + 4h^2 y^2 - y^4\right)}{8h^3}. \tag{4}$$

Obviously, a Hydrogen-like atomic motion described by the Hamiltonian

$$\hat{H}_z \approx \frac{\hat{p}_z^2}{2m} - \frac{\Lambda e^2}{4\pi \varepsilon_0 z} + e E_{dc} z, \tag{5}$$

with m being the mass of the electron and $\hat{p}_z$ the momentum operator, can be obtained [19, 20] for the trapped electron vibrating along the direction perpendicular to the liquid surface. As the transition frequency (which is in the MMW band) between the lowest two energy levels of such a Hydrogen-like atom is much higher than the vibrational frequency (which is in the CMW band) of the trapped electron vibrating along the y-direction parallel to liquid Helium surface, the vertical motion of the trapped electron can be safely neglected for the manipulations of the lateral motion.

Furthermore, in the present configuration shown in Fig. 1, the $x-$direction motion of the trapped electron is limited within a spacing of 20 μm, which is far less than its vibrational wavelength on the order of centimeters. As a consequence, the vibration of the trapped electron along the x-direction can be safely neglected. Therefore, only the y-direction vibration of the trapped electron can be considered. Besides the potential generated by the voltage-biased electrode, a standing wave electric field generated by the CPW-TLR can also be utilized to trap the electron on liquid Helium. As a result, the y-direction vibration of the trapped electron can be described by an anharmonic potential. The Hamiltonian describing the y-direction vibration of the trapped electron can be approximated as

$$\hat{H}_a \approx \frac{\hat{p}_y^2}{2m} + U_y, \ \ U_y = \frac{e E_{dc}}{2h} y^2 - \frac{e E_{dc}}{8h^3} y^4. \tag{6}$$

Obviously, it describes a one-dimensional nonlinear vibration; a linear harmonic oscillator $\hat{H} = \hat{p}^2/(2m) + m\omega_y^2 y^2/2$ with a vibrational frequency: $\omega_y = \sqrt{e E_{dc}/(mh)}$, plus a nonlinear term $\sim y^4$. In the representation of the number of linear vibrational phonons, the Hamiltonian (6) can be further expressed as:
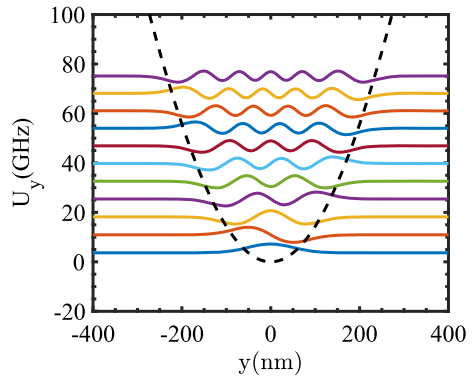
$$\hat{H}_a' = \hbar\omega_y \left(\hat{a}^\dagger \hat{a} + \frac{1}{2}\right) - \frac{\hbar^2}{32mh^2} (\hat{a} + \hat{a}^\dagger)^4. \tag{7}$$

Here, $\hbar$ is Planck constant, $\hat{a}$ ($\hat{a}^\dagger$) is the Bosonic annihilation (creation) operator of the vibrational phonon and $[\hat{a}, \hat{a}^\dagger] = 1$.

Under the first-order approximation, the eigenvalue of the Hamiltonian (6) can be easily obtained as

$$E_n = \langle n|\hat{H}_a'|n\rangle \approx \hbar\omega_y \left(n + \frac{1}{2}\right) - \frac{3\hbar^2(2n^2 + 2n + 1)}{32mh^2}, \tag{8}$$

for the eigenstate $|n\rangle$, $n = 0, 1, 2, 3, \ldots$. Figure 2 shows the y-dependent potential of the nonlinear vibration and the corresponding stationary wave functions of the trapped electron.

Specifically, if the thickness of liquid Helium and the strength of the electrostatic field are, respectively, set typically as $h = 500$ nm and $E_{dc} = 53.87$ V/cm, then the frequency of the linear vibration of the electron along the y-direction is calculated as $f_y = \omega_y/(2\pi) = \sqrt{eE_{dc}/(mh)}/(2\pi) \approx 6.93$ GHz, which is much lower than the frequency of the Hydrogen-like atomic vibration along the direction perpendicular to the liquid Helium surface. Therefore, the vertical z-direction vibration is safely decoupled from that of the lateral y-direction. The energy of the vibrational ground state and the first excited one of such a nonlinear harmonic oscillator are, respectively, calculated as: $E_0 = \hbar\omega_y/2 - 3\hbar^2/(32mh^2) \approx 14.30$ μeV, and $E_1 = 3\hbar\omega_y/2 - 15\hbar^2/(32mh^2) \approx 42.83$ μeV, with the transition frequency between them being: $\omega_a = (E_1 - E_0)/\hbar \approx 2\pi \times 6.90$ GHz, which is close to the experimental observation [22, 36].

The above calculation indicates that the lowest two energy stationary states: $|0\rangle$ and $|1\rangle$, of this nonlinear harmonic oscillator, can be utilized to encode the desired qubit

$$\hat{H}_a'' = \frac{1}{2}\hbar\omega_a\hat{\sigma}^z, \, \hat{\sigma}^z = |1\rangle\langle1| - |0\rangle\langle0| \tag{9}$$

whose eigenfrequency is really in the CMW band. Compared with the MMW band microwave pulses required to implement the quantum manipulations of the Hydrogen-like atomic qubits [19], the technique by using the microwave pulses in MMW band to manipulate the present qubit is developed well and has been widely applied in the current solid-state circuit QED systems [37].

2.2 Qubit level stability

In this subsection, we confirm that the proposed qubit encoded by the two lowest levels of the anharmonic oscillator is sufficiently stable, i.e., the qubit leakages could be safely neglected.
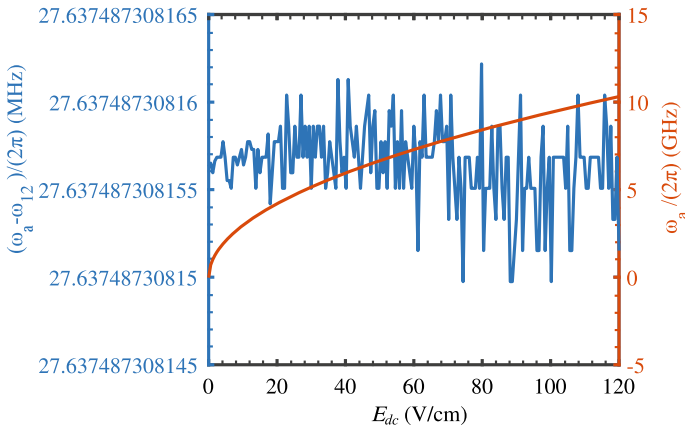
Fig. 3 The transition frequency $\omega_a = (E_1 - E_0)/\hbar$ and the difference between ω_a and the transition frequency $\omega_{12} = (E_2 - E_1)/\hbar$ versus the trapping static electric field strength E_{dc}. Here, the red line refers to $\omega_a/(2\pi)$ (with the unit being GHz) and the blue curve refers to $(\omega_a - \omega_{12})/(2\pi)$ (with the unit being MHz), and E_j is the energy of the j-th ($j = 0, 1, 2$) created level of the y-direction anharmonic oscillation of the trapped electron

First, besides the environment noises the strength fluctuation of the transverse trapping static electric field E_{dc} might influence the energy level distribution of the trapped electron vibrating along the y-direction. However, as shown in Fig. 3, although the transition frequency ω_a of the qubit changes really with the E_{dc} (red line),

it really be isolated from the transition frequency, i.e., $\omega_a - \omega_{12} = (E_2 - E_1)/\hbar \sim 27.64$ MHz, where E_2 is the energy of the third level of the anharmonic oscillator. This implies that, during the qubit operation by using the narrow linewidth (such as a few MHz) microwave pulse, the possible qubit leakage can be suppressed robustly.

Next, we verify that the qubits in a trap array are addressable individually, although the Coulomb interactions between the electrons in different traps are always on. Basically, the high-fidelity single-qubit operation is desirable for the scalable quantum computing on chip. In the present configuration shown typically in Fig. 1, the Coulomb interaction of the electrons trapped in two adjacent potentials can be easily expressed as

$$U_{ee} = \frac{e^2}{4\pi\varepsilon_0 S},\tag{10}$$

where $S = Y_{n+1} - Y_n + y_n + y_{n+1}$ is the distance between the electrons with Y_n being the equilibrium position of the electron trapped in the n-th potential, in which the vibrational displacement of the electron away from its equilibrium position is y_n. Experimentally, the distance between the centers of two nearest-neighbor potentials could be set as: $S_y = Y_{n+1} - Y_n \sim 100\,\mu$m, yielding $y_n/S_y \ll 1$. As a consequence, by neglecting the higher-order terms of y_n/S_y, Eq. (10) reduces to

$$U_{ee} = \frac{e^2}{4\pi\varepsilon_0(S_y + y_n + y_{n+1})}$$

$$\approx \frac{e^2}{4\pi\varepsilon_0 S_y}\left[1 + \frac{y_n^2 - y_n S_y}{S_y^2} + \frac{y_{n+1}^2 - y_{n+1} S_y}{S_y^2} + \frac{2y_n y_{n+1}}{S_y^2}\right]. \quad (11)$$

Here, the first term is a c-number term which can be omitted certainly. The second and third terms represent the negligible Stark shifts of the levels. Therefore, the interaction between the electrons trapped in different potentials is mainly determined by the fourth term. In the phonon representation, the Coulomb interaction between the electrons trapped in the nearest-neighbor potentials can be effectively expressed as

$$\hat{H}_{ee} = \frac{2e^2 y_n y_{n+1}}{4\pi\varepsilon_0 S_y^3} \approx \hbar g_{ee}(\hat{c}_n\hat{c}_{n+1}^\dagger + \hat{c}_n^\dagger\hat{c}_{n+1}), \quad (12)$$

under the usual rotating wave approximation. Here, $g_{ee} \approx e^2/(4\pi\varepsilon_0 m S_y^3\omega_y)$ is the strength, $\hat{c}_n$ ($\hat{c}_n^\dagger$) is the vibrational Bosonic annihilation (creation) operator of the n-th electron and $[\hat{c}_n, \hat{c}_n^\dagger] = 1$. With the typical parameters, such as $E_{dc} = 53.87$ V/cm, $S_y \sim 100\ \mu$m, and $\omega_y \sim 2\pi \times 6.93$ GHz, we get $g_{ee} \sim 2\pi \times 0.93$ KHz. This implies that the Coulomb interaction between the electrons trapped in the nearest-neighbor traps along the y-direction is significantly weak, i.e., it does not yield the uncontrolled qubit–qubit interaction, and thus, the arbitrarily selected qubits could be addressed individually. Indeed, we can further verify that, comparing with the coupling between the qubit and the CPW-TLR at the bottom of liquid Helium, the Coulomb interaction between the qubits can be really neglected. This can be further verified by compared it with the qubit-TLR interaction:

$$\hat{H}_I = e\hat{d}\hat{E}_{rf}(y), \quad (13)$$

with

$$\hat{E}_{rf}(y) = \frac{\hat{V}(y)}{h} = \frac{k}{C}\cos(ky)\sqrt{\frac{\hbar}{Ll\omega_r}}(\hat{a}_r + \hat{a}_r^\dagger) \quad (14)$$

being the electric field in the resonator [37–40]. In the qubit representation spanned by $|0\rangle$ and $|1\rangle$, we have

$$\hat{d} = (|0\rangle\langle0| + |1\rangle\langle1|)\ y\ (|0\rangle\langle0| + |1\rangle\langle1|) = \sum_{i,j=0,1} y_{ij}|i\rangle\langle j|, \quad (15)$$

where $\langle i|y|j\rangle = \int \psi_i y\psi_j^* dy$ and $i \neq j = 0, 1$, with $\psi_{i,j}$ being the relevant qubit wave functions. With the typical parameters, one can easily prove that, $y_{01} = y_{10} \sim 3.65 \times 10^{-8}$ m$\gg y_{00} \sim 2.32 \times 10^{-22}$ m, and $y_{11} \sim 3.35 \times 10^{-22}$ m. Therefore, the
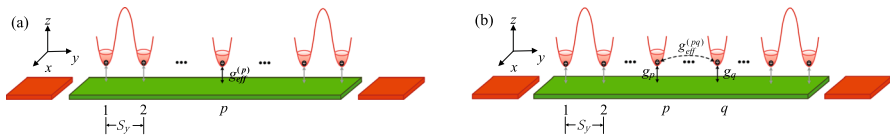
Fig. 4 A qubit array is generated by a series of trapped electrons on liquid Helium to implement the desired quantum computation. Here, the qubit is encoded by the ground- and first excited state of the vibration of the trapped electron along the y-direction, and the CPW-TLR is served as the data bus to implement the operation(s) on the addressable qubit(s). The other qubits are adjusted to far-off resonant interaction with the CPW-TLR and thus cannot be driven. **a** Individually addressable single-qubit operation on the arbitrarily selected the pth qubit by adjusting its eigenfrequency to implement the resonant interaction with the CPW-TLR. **b** Tunable two-qubit operation on the arbitrarily addressed two qubits, e.g., the p-th- and q-th ones, by using the effective interaction between them

y-dependent interaction between the qubit and the transverse quantized electric field in the CPW-TLR can be expressed as:

$$\hat{H}_I(y) = \hbar g_{eR}(\hat{a}_r\hat{\sigma}^+ + \hat{a}_r^\dagger\hat{\sigma}^-). \tag{16}$$

Here, $\hat{\sigma}^+ = |1\rangle\langle 0|$ and $\hat{\sigma}^- = |0\rangle\langle 1|$ are the pseudo-spin Pauli operators of the qubit. For the designed parameters in Fig. 1(b), we have $\omega_r \approx 2\pi \times 5.70$ GHz for $l = 11063~\mu$m, $Z_0 \approx 55.40~\Omega$, $C \approx 1.57$ pF, and $L = 4.82$ nH. For $y \sim 4900~\mu$m, the value of the $g_{eR}(y)$-parameter in Eq. (16) can be estimated as: $g_{eR} = [ey_{01}\cos(ky)/h]\sqrt{1/(C^2Ll\hbar\omega_r)} \approx 2\pi \times 14.92$ MHz. This indicates that the qubit-TLR coupling is still sufficiently weak, compared with the qubit leakage frequency, i.e., $\omega_a - \omega_{12} \sim 2\pi \times 27.64$ MHz. However, it is significantly larger than the Coulomb interaction (i.e., $g_{ee} \sim 2\pi \times 0.93$ KHz) between the electrons in the adjacent traps along the y-direction. Therefore, both the Coulomb interaction between the electrons in different traps and the coupling of the qubit with the CPW-TLR do not lead to the unwanted qubit leakages. The CPW-TLR can thus be served as the data bus to implement the desired single-qubit rotation, switchable two-qubit coupling, and also the readouts of the qubits.

It is valuable to emphasize that two main points are considered for the chip designs. First, the coupling strength g_{eR} should be sufficiently weak to satisfy the rotating wave approximation condition. Secondly, the indirect qubit–qubit interaction generated by using the resonator as a data bus should be sufficiently strong for the implementations of various qubit manipulations. With the above numerical estimations, we argue that a qubit array with at least 20 traps (with a spacing of $100~\mu$m) can be generated on liquid Helium. Certainly, the size of the array can be further improved, at least theoretically.

3 The feasibility of the basic quantum gate operations

With the designs demonstrated above, we now discuss how to implement the desired gate operations for quantum computation with the qubit array being specifically shown in Fig. 4.

The well-developed circuit QED technique, used widely for superconducting quantum computation, can be directly applied to implement the desired quantum gate operations with the present system, although certain details are still required to be considered specifically. First, in the circuit QED system the qubit and the cavity are in the same plane, for example, the vacuum electric field of the cavity can be directly coupled to the qubit by providing a biased voltage and flux [37], while, in the present system, the cavity at the bottom of the liquid Helium and the qubits encoded by the lateral orbit states of the trapped electrons are not in the same plane, and thus the qubit–cavity interaction is gotten by the direct electric-dipole one of the electrons in the vacuum electric field. Second, the interaction between the distant qubits in the superconducting circuit QED chip can be switched on/off by either adjusting their detunings with the commonly coupled cavity or using the switchable couplers, while, in the present system the interbit interaction includes additionally the always-on electron–electron Coulomb couplings; therefore, it is furthermore required to treat these interactions and evaluate their influences on the implementations of high-fidelity single-qubit gate operations. Thirdly, differing from the qubits in the superconducting circuit, the present qubits possess basically longer decoherence times, as the liquid Helium might isolate most of the circuit noises and thus only the ripplons [21] on the liquid Helium surface are the key source of the unwanted decoherence. Therefore, the quantum computation with the present qubits might possess more advantages over that with the superconducting qubits in the circuit QED system; at least the longer durations of the applied pulses can be applied to implement the desired gate operations and the higher-fidelity readouts of the qubit.

3.1 Single-qubit gate operations on the addressed qubit

Let us first discuss the feasibility of the single-qubit operation on the arbitrarily addressable qubit, such as the p-th one, by driving the CPW-TLR, shown schematically in Fig. 4a. As the eigenfrequency ω_a of the qubit can be adjusted individually by controlling the trapping electric fields via the electrodes at the bottom of liquid Helium, and also the influence of the Coulomb interactions between the selected qubit and the other ones in different potentials can be safely neglected, the arbitrarily selected qubit can be addressed by letting it couple to the CPW-TLR, individually. The other qubits are decoupled simultaneously by letting their frequencies be far-off resonance with the CPW-TLR.

The Hamiltonian for driving the CPW-TLR to couple it to the p-th qubit can be written as [41]:

$$\hat{H}_p = \hbar\omega_r \hat{a}_r^\dagger \hat{a}_r + \frac{1}{2}\hbar\omega_p \hat{\sigma}_p^z + \hbar g_p(\hat{a}_r^\dagger \hat{\sigma}_p^- + \hat{a}_r \hat{\sigma}_p^+) + \hbar\hat{a}_r \xi^* e^{i\omega_d t} + \hbar\hat{a}_r^\dagger \xi e^{-i\omega_d t}.$$

(17)

where $\hat{\sigma}_p^z$, $\hat{\sigma}_p^+$ and $\hat{\sigma}_p^-$ are the pseudo-spin Pauli operators of the p-th qubit. Here, the first and the second terms are the free Hamiltonians of the quantized microwave standing wave field in the CPW-TLR and the selected qubit, respectively. The third term

refers to the interaction between the qubit and the CPW-TLR under the usual rotating wave approximation, wherein the strength $g_p = g_{eR}(y_p)$ depends on the location of the p-th qubit; the last two terms describe the microwave drive of the CPW-TLR with ω_d and ξ being the driving frequency and strength, respectively. Interestingly, the Hamiltonian (17) undergoes an evolution

$$
U_p(t) = \begin{pmatrix} \cos\left[\frac{A(t)}{2}\right] & -i\sin\left[\frac{A(t)}{2}\right] \\ -i\sin\left[\frac{A(t)}{2}\right] & \cos\left[\frac{A(t)}{2}\right] \end{pmatrix},
\tag{18}
$$

which is nothing but a single-qubit operation of the p-th qubit. By adjusting the driving strength $\alpha(t)$ and the driving time t, various single-qubit state manipulations can be specifically achieved. For example, if $A(t) = \pi$, then the single-qubit X gate: σ_p^X, can be realized, while if $A(t) = \pi/2$, then the Hadamard gate operation on the p-th qubit can be realized. Actually, if the frequency of another qubit is set as $\omega_{ot} = 10$ GHz, the effective couple strength $g_{ot}^2/(\omega_{ot} - \omega_r)$ between it and CPW-TLR reads ~ 0.21 MHz, which is much less than $g_{eR}^2/(\omega_p - \omega_r) \sim 1.17$ MHz. Therefore, the coupling between the driven CPW-TLR and the other qubits can be effectively neglected by engineering their frequencies to be far-off resonances by controlling their static electric field biases.

3.2 Two-qubit logic gate on a pair of arbitrarily selected qubits

Next, we investigate how to implement the two-qubit operation between a pair of arbitrarily qubits by using the tunable inter-qubit interaction achieved by using the simultaneously coupling them to the data bus, i.e., the CPL-TLR. As shown in Fig. 4b, the p-th and q-th of the frequencies ω_p and ω_q, with the negligible Coulomb interaction, are addressed to simultaneously couple to the CPW-TLR. The Hamiltonian for such an operation reads

$$
\hat{H}_{do} = \hbar\omega_r \hat{a}_r^\dagger \hat{a}_r + \frac{1}{2}\hbar\omega_p \hat{\sigma}_p^z + \frac{1}{2}\hbar\omega_q \hat{\sigma}_q^z + \hbar g_p(\hat{a}_r^\dagger \hat{\sigma}_p^- + \hat{a}_r \hat{\sigma}_p^+) + \hbar g_q(\hat{a}_r^\dagger \hat{\sigma}_q^- + \hat{a}_r \hat{\sigma}_q^+),
\tag{19}
$$

where σ_q^z, σ_q^+ and σ_q^- are the pseudo-spin Pauli operators of the q-th qubit. g_p and $g_q = g_{eR}(y_q)$ are dependent of the locations of the qubits. Under the conditions: $g_p \ll \Delta_p$, and $g_q \ll \Delta_q = |\omega_q - \omega_r|$, the Hamiltonian (19) can be effectively written as:

$$
\begin{aligned}
\hat{H}'_{do} = &\hbar(\omega_r + \chi_p \hat{\sigma}_p^z + \chi_q \hat{\sigma}_p^z)\hat{a}_r^\dagger \hat{a}_r + \frac{1}{2}\hbar(\omega_p + \chi_p)\hat{\sigma}_p^z + \frac{1}{2}\hbar(\omega_q + \chi_q)\hat{\sigma}_p^z \\
&+ \hbar g_{eff}^{(pq)}(\hat{\sigma}_p^- \hat{\sigma}_q^+ + \hat{\sigma}_p^+ \hat{\sigma}_q^-),
\end{aligned}
\tag{20}
$$

where $\chi_p = 2g_p^2/\Delta_p$, $\chi_q = 2g_q^2/\Delta_q$, and

$$g_{eff}^{(pq)} = \frac{g_p g_q (\Delta_p + \Delta_q)}{\Delta_p \Delta_q} \qquad (21)$$

is the effective interaction between the distant qubits. Above, the second- and higher orders of g_p/Δ_p and g_q/Δ_q are ignored. It indicates that an effective interaction $g_{eff}^{(pq)}$ between the p-th- and q-th qubits without the direct interaction can be obtained by using the CPL-TLR as the data bus.

Specifically, if $\Delta_q = \Delta_p = \Delta$ and $g_p = g_q = g$, then the effective coupling Hamiltonian between the distant qubits can be abbreviated as:

$$\hat{H}_{qp} = \frac{2\hbar g^2}{\Delta}(\hat{\sigma}_p^- \hat{\sigma}_q^+ + \hat{\sigma}_p^+ \hat{\sigma}_q^-), \qquad (22)$$

in the interaction picture. It delivers the following evolution operator:

$$U_{qp}(t) = \exp(-\frac{i}{\hbar}\hat{H}_{qp}t) = \begin{pmatrix} 1 & 0 & 0 & 0 \\ 0 & \cos(\kappa t) & -i\sin(\kappa t) & 0 \\ 0 & -i\sin(\kappa t) & \cos(\kappa t) & 0 \\ 0 & 0 & 0 & 1 \end{pmatrix}, \qquad (23)$$

with $\kappa = 2g^2/\Delta$. Obviously, when the evolution time is controlled as $t = \pi/(2\kappa)$, a two-qubit i-SWAP gate operation between the distant qubits can be realized. It is emphasized that the effective coupling between the selected two qubits could be realized. One can see from Eq. (22) that the effective interaction between the qubits can be engineered by adjusting the eigenfrequencies of the qubits and consequently the detunings between them the TLR. For instance, by setting $\omega_p = \omega_q = 2\pi \times 6.90$ GHz, the virtual interaction strength between two qubits can be obtained as $g_{eff}^{(pq)} \sim 2.33$ MHz, which is significantly stronger than the Coulomb interaction between the two trapped electrons.

Certainly, the implementation of the desired high-fidelity two-qubit gates is required to suppress the cross-talks from the other qubits. For example, the influence from the third qubit, says the sth one, on the fidelity of the desired two-qubit gate operation between the selected p-th and q-th ones. This is certainly feasible, at least theoretically, by setting the eigenfrequency of the s-th qubit to be large detuning from the selected qubits. Neglecting all the significantly weak Coulomb interactions, the Hamiltonian for the coupled three-qubit system, say p, q, and s, by the common CPW-TLR, can be specifically written as

$$\begin{aligned} \hat{H}_{tri} =& \hbar\omega_r \hat{a}_r^\dagger \hat{a}_r + \frac{1}{2}\hbar\omega_p \hat{\sigma}_p^z + \frac{1}{2}\hbar\omega_s \hat{\sigma}_s^z + \frac{1}{2}\hbar\omega_q \hat{\sigma}_q^z + \hbar g_p(\hat{a}_r^\dagger \hat{\sigma}_p^- + \hat{a}_r \hat{\sigma}_p^+) \\ &+ \hbar g_s(\hat{a}_r^\dagger \hat{\sigma}_s^- + \hat{a}_r \hat{\sigma}_s^+) + \hbar g_q(\hat{a}_r^\dagger \hat{\sigma}_q^- + \hat{a}_r \hat{\sigma}_q^+). \end{aligned} \qquad (24)$$
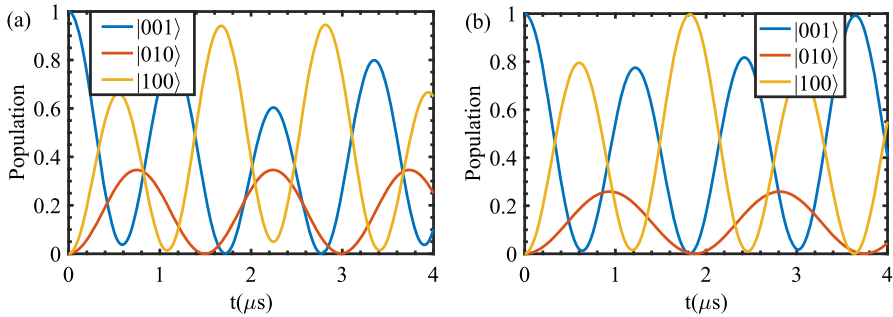
Fig. 5 Numerical simulations of the population evolutions of the two-qubit i-SWAP gate operation: $|001\rangle \leftrightarrow |100\rangle$, under the presence of the middle qubit prepared initially at the state $|0\rangle$. The blue, red, and yellow lines refer to the states $|001\rangle$, $|010\rangle$, and $|100\rangle$, respectively. Here, the eigenfrequencies of the first and third qubits are set as $\omega_p/(2\pi) = \omega_q/(2\pi) = 6.90$ GHz, while that of the second qubit, i.e., the middle one, is set as $\omega_s/(2\pi) = 10$ GHz (**a**) and $\omega_s/(2\pi) = 16$ GHz (**b**), respectively

Under the condition: $g_s/\Delta_s, g_p/\Delta_p, g_q/\Delta_q \ll 1$, it can be effectively rewritten as:

$$\hat{H}^I_{tri} = \hbar g_{ps}(\hat{\sigma}^-_p\hat{\sigma}^+_s + \hat{\sigma}^+_p\hat{\sigma}^-_s) + \hbar g_{pq}(\hat{\sigma}^-_p\hat{\sigma}^+_q + \hat{\sigma}^+_p\hat{\sigma}^-_q) + \hbar g_{sq}(\hat{\sigma}^-_s\hat{\sigma}^+_q + \hat{\sigma}^+_s\hat{\sigma}^-_q),$$

(25)

in the interaction picture, where

$$g^{(ps)}_{eff} = \frac{g_p g_s(\Delta_p + \Delta_s)}{\Delta_p \Delta_s}, \quad g^{(sq)}_{eff} = \frac{g_s g_q(\Delta_s + \Delta_q)}{\Delta_s \Delta_q},$$

(26)

and $\Delta_s = |\omega_s - \omega_r|$. Therefore, the influence of the s-th qubit, on the fidelity of the desired two-qubit i-SWAP gate operation between the selected p-th and q-th ones, can be numerically checked the state evolution of the three-qubit system using the time-evolution operator $U_{tri} = \exp(-\frac{i}{\hbar}\hat{H}^I_{tri}t)$. Figure 5 specifically shows how the populations of the state $|001\rangle$ change with the different pulse duration.

One can see that, for $\omega_s = 2\pi \times 10$ GHz and $g^{(ps)}_{eff} \sim 1.24$ MHz, if the duration is set as $t = \pi/(2\kappa) \sim 0.67$ μs, the populations read 0.08 for the state $|001\rangle$, 0.34 for the state $|010\rangle$, and 0.58 for the state $|100\rangle$, respectively. This indicates that the fidelity of the i-SWAP gate is lowered manifestly as 58%. However, if the duration of the applied is enlarged as 1.67μs, then the fidelity of the two-qubit i-SWAP gate can be further enhanced up to 94.12%. In fact, as shown in Fig. 5b, such a fidelity can be significantly enhanced, e.g., up to 99.99%, if the detuning between the s-th qubit and the $p - /q$-th qubit can be further enlarged. Therefore, by enhancing the detunings and also properly setting the duration of the applied microwave pulses, the desired two-qubit gate operations can be implemented with high fidelities, even if the other qubits are practically in the presence.

Theoretically, with the combination of the single-qubit operations on the arbitrarily addressable qubits and a tunable two-qubit quantum logic gate operation on the arbitrarily selected two qubits, any quantum operation can be achieved to implement the

desired quantum computation. Therefore, with the quantum gate operations demonstrated above, quantum computation with the qubits encoded by the lateral vibrations of the trapped electrons on liquid Helium is feasible.

4 Numerical confirmations of the QND readouts of the qubits

In fact, due to the controllable dispersive interaction, the QND measurements of the arbitrarily selected qubit can be implemented by probing the transmission of the driving microwave. This method has been widely applied to various solid-state circuit QED systems [42–45]. We demonstrate the QND readout(s) of the arbitrarily selected qubit(s) by numerical simulations and indicate it is feasible for the present one.

Specifically, the QND readout the p-th qubit, by using the microwave to drive the dispersively coupled CPW-TLR, can be described by the following Hamiltonian [46]:

$$
\begin{aligned}
\hat{H}_p =& \frac{1}{2}\hbar\omega_p\hat{\sigma}_p^z + \hbar\omega_r\hat{a}_r^\dagger\hat{a}_r + \frac{\hbar g_p^2}{\triangle_p}\hat{a}_r^\dagger\hat{a}_r\hat{\sigma}_p^z + \sum_{n=1,2}\int_{-\infty}^{+\infty}\hbar\omega_n d\omega_n\hat{b}_n^\dagger(\omega_n)\hat{b}_n(\omega_n) \\
&+ i\hbar\sum_{n=1,2}\int_{-\infty}^{+\infty}d\omega_n\lambda_n(\omega_n)\left[\hat{a}_r\hat{b}_n^\dagger(\omega_n) - \hat{a}_r^\dagger\hat{b}_n(\omega_n)\right],
\end{aligned}
\tag{27}
$$

where $\hat{b}_n(\omega_n)$ ($n = 1, 2$) and $\hat{b}_n^\dagger(\omega_n)$ are the operators of the applied microwave pulse with the frequency ω_n, λ_n is the interaction strength between it and CPW-TLR, the detected qubit is dispersively coupled to the driven CPW-TLR and thus $\triangle_p \gg g_p$.

For the detection, the dissipation rate of the qubit is assumed to be sufficiently lower than that of the driven CPW-TLR, and thus, the qubit dissipation is negligible, i.e., $\hat{\sigma}_p^z(t) = \hat{\sigma}_z(0)$ in Heisenberg picture, to keep the population of the qubits be unchanged during its readouts. Using the standard input–output theory [46], the transmission coefficient of the microwave-driven CPW-TLR can be easily calculated as:

$$
t_p(\omega) = \frac{\sqrt{\gamma_1\gamma_2}}{\frac{1}{2}(\gamma_1 + \gamma_2) + i[\frac{g_p^2}{\triangle_p}\langle\hat{\sigma}_p^z(0)\rangle - (\omega - \omega_r)]}.
\tag{28}
$$

where $\gamma_n = 2\pi\lambda_n^2$ is the dissipation of bilateral mirrors of the resonator cavity. It is seen from Fig. 6 that, compared with spectrum of the empty cavity (EMC) peaked at $\omega = \omega_r$, if the qubit is in the excited (ground) state, the peak of the transmitted spectrum is shifted $g_p^2/\triangle_p = 1.16$ MHz to the right (left) from the central frequency ω_r. With the current parameter settings, it is easy to distinguish curves of different states.

Besides the above frequency domain measurements, there is also implementing the time domain detections of the qubit by using the usual IQ-mixing technique.

The IQ-mixing technique is usually performed as follows. First, a microwave signal $E_{LO} = A_{LO}\sin(\omega_{LO}t)$, with a known frequency and amplitude, is divided into two channels by a power divider; one is served as the local coherent signal, and the other is used to drive the CPW-TLR for the detection. Next, if the TLR is coupled to the qubit
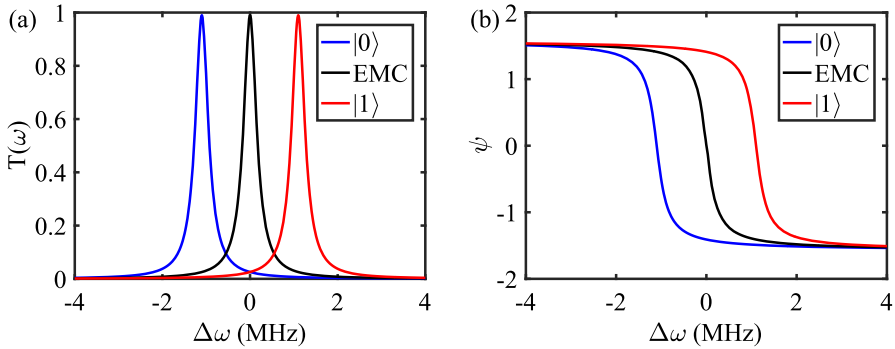
Fig. 6 Microwave transmission spectra of the driven CPW-TLR dispersively coupled to the detected q-th qubit, whose different states lead to the different shifts of the peak: **a** is the transmission intensity spectrum, **b** is the transmission phase-shift spectrum. Here, the black line refers to the EMC, and the blue (red) line peaked at $\triangle\omega_{|0_p\rangle} = -g_p^2/\triangle_p = -1.16$ MHz ($\triangle\omega_{|1_p\rangle} = g_p^2/\triangle_p = 1.16$ MHz) corresponding to the qubit is in the ground (excited) state. The relevant parameters are set as: $\omega_p/(2\pi) = 6.90$ GHz and $\omega_r/(2\pi) = 5.70$ GHz, $g_p/(2\pi) = 14.91$ MHz, $\gamma_1/(2\pi) = 25.65$ KHz, and $\gamma_2/(2\pi) = 31.35$ KHz, respectively

wanted to be readout, then its transmitted signal reads: $E_{out}(t) = A_i \cos(\omega_{LO}t + \phi_i)$ ($i = 0, 1$), depending on the states of the qubit. Finally, by mixing the local and transmitted signals, the qubit-induced changes, i.e., A_i and ϕ_i, can be determined as:

$$A_i = \left| \frac{\langle \hat{a}_{out}^{(2)} \rangle}{\langle \hat{a}_{in}^{(1)} \rangle} \right|, \quad \phi_i = \arctan\left(\frac{\langle \hat{a}_{out}^{(2)} \rangle}{\langle \hat{a}_{in}^{(1)} \rangle} \right). \tag{29}$$

They can be determined by simultaneously probing the signals at the I-part outport [45, 47]:

$$S_I = E_{LO}^{(1)} \times E_{out}^{(I)} \approx \frac{A_{LO}A_i}{4} \cos\phi_i, \tag{30}$$

and the Q-part one:

$$S_Q = E_{LO}^{(2)} \times E_{out}^{(Q)} \approx \frac{A_{LO}A_i}{4} \sin\phi_i. \tag{31}$$

Above, the high-frequency signals generated by the mixer are filtered out.

Certainly, noise always exists in the actual experimental measurements and thus affects the measurement accuracies of the I- and Q-signals. Figure 7 numerically simulates how the statistical distributions of the measured I–Q signals for 1000 measurements on a given qubit state. It is seen that, when the qubit is prepared at the $|0_p\rangle$-state, the signal amplitudes are basically distributed near a yellowed center point located at $(S_I, S_Q)=(0.97, 0.17)$, while if the qubit state is prepared at the $|1_p\rangle$-state, the signal amplitudes are alternatively distributed around another yellowed center point located at $(S_I, S_Q) = (0.97, 0.16)$. Correspondingly, Fig. 7(b) shows that, if the qubit
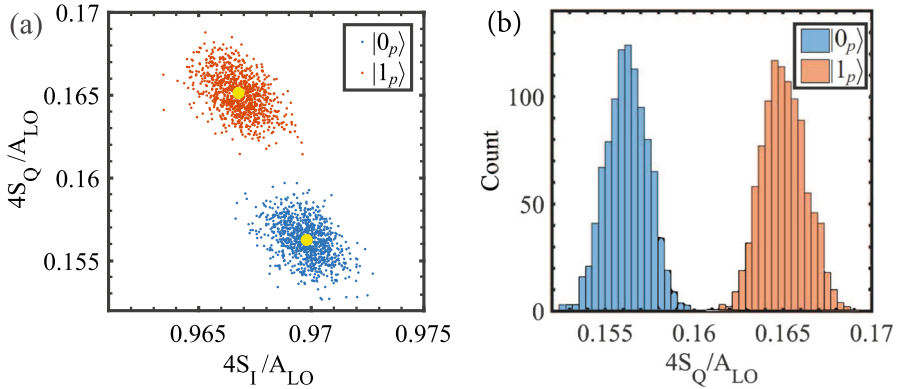
Fig. 7 Simulation of time-domain measurements of the selected p-th qubit by using the IQ-mixing technique: **a** the distribution of the measured signals on the I-Q plane; the blue (red) dots refer to the qubit in the ground state $|0_p\rangle$ (the excited state $|1_p\rangle$), wherein the yellow dots correspond to the ideal distributions; **b** the statistical distribution of the measured I-Q signals shows that, for the same measurement samples, the heights of the statistical peaks are basically the same. Here, the parameters are set as the same as in Fig. 6

is prepared at either the state $|1_p\rangle$ or $|0_p\rangle$, the number of the events that the measured (I, Q) values near one of the yellowed center points is almost the same.

Experimentally, both the frequency domain and time domain QND measurement of the qubit can be implemented, if the dissipation time of the detected qubit is significantly longer than the transmitted one of the driving microwave through the TLR with the sufficiently wide linear regions [48].

5 Conclusion

In summary, we have proposed an approach to implement the quantum computation with the qubits encoded by the nonlinear lateral vibrations of the electrons being trapped on liquid Helium. The eigenfrequency of the present qubit is in the CMW band rather than the MMW one in the previous scheme for the quantum computation with surface-state electrons on liquid Helium. Thus, the technique used widely in the circuit QED systems can also be directly applied to manipulate the present qubits. The stability of such a qubit, against the perturbations of the electron–electron Coulomb interactions and the qubit–TLR interaction, had been analyzed, in detail. Interestingly, the scheme is scalable. Furthermore, with the quantized field in the CPW-TLR as the data bus, the arbitrarily selected qubit can be addressed individually to implement the single-qubit operation, and the effective interaction between a pair of arbitrarily selected qubits is tunable for the implementation of the two-qubit quantum gate operation. Also, the CPW-TLR can be served as the detector for the QND measurements of the qubit, in both the frequency and time domains. By the relevant numerical simulations, we demonstrated that the quantum computation with the arrayed qubits, generated by the nonlinear lateral vibrations of the electrons on liquid Helium, is possible.

For the experimental realization, a series of setups have been built to implement the trap of the electrons on liquid Helium and even on the solid Neon [44]. Specifically, it has been demonstrated experimentally that the lateral vibration parallel to the Helium surface is nonlinear [22]. Also, the electron trap on liquid Helium can be integrated with a superconducting coplanar cavity device on a chip, and the MHz-order coupling strength (which is much larger than the resonator linewidth) has been experimentally demonstrated. Moreover, the duration $(\pi/(2\kappa))$ of the proposed π-pulse for the implementation of the two-qubit operation is estimated as the μs-order, which is feasible. Typically, if the intensity of the static electric field is set as 5387 V/m, and the width of the electrode is 100 μm, the static voltage for trapping the electron can be calculated as $\sim$ 0.5387 V. It is realizable. In addition, at a sufficiently low temperature $\sim$ 15 mK, the environment thermal noise could be safely suppressed. Hopefully, the feasibility of the scheme demonstrated numerically here can be experimentally verified soon.

Author Contributions Y. L. wrote the main manuscript and prepared all figures. Y. L. and S. H. investigated the background of the study. S. H. tested the theoretical correctness of the article. M. Z. put forward the suggestions of Eq. (3) and (10). L. W. proposed the design scheme, edited the manuscript, and provided funding acquisition. All authors reviewed the manuscript.

Data availability No datasets were generated or analysed during the current study.

Declarations

Conflict of interest The authors declare that they have no conflict of interest.

References

1. Coccia, M.: Disruptive innovations in quantum technologies for social change. J. Econ. Bib. **9**, 21 (2022)
2. Arute, F., Arya, K., Babbush, R., et al.: Quantum supremacy using a programmable superconducting processor. Nature **574**, 505 (2019)
3. Zhong, H.S., Wang, H., Deng, Y.H., et al.: Quantum computational advantage using photons. Science **370**, 1460 (2020)
4. Barends, R., Shabani, A., Lamata, L., et al.: Digitized adiabatic quantum computing with a superconducting circuit. Nature **534**, 222 (2016)
5. Inagaki, T., Inaba, K., Hamerly, R., et al.: Large-scale Ising spin network based on degenerate optical parametric oscillators. Nat. Photon. **10**, 415 (2016)

6. Mcmahon, P.L., Marandi, A., Haribara, Y., et al.: A fully programmable 100-spin coherent Ising machine with all-to-all connections. Science **354**, 614 (2016)
7. Martinis, J.M., Devoret, M.H., Clarke, J.: Quantum Josephson junction circuits and the dawn of artificial atoms. Nat. Phys. **16**, 234 (2020)
8. Criac, J.I., Zoller, P.: Quantum computations with cold trapped ions. Phys. Rev. Lett. **74**, 4091 (1995)
9. Monroe, C., Meekhof, D.M., King, B.E., et al.: Demonstration of a fundamental quantum logic gate. Phys. Rev. Lett. **75**, 4714 (1995)
10. Sackett, C.A., Kielpinski, D., King, B.E., et al.: Experimental entanglement of four particles. Nature **404**, 256 (2000)
11. Schmidt-Kaler, F., Häffner, H., Riebe, M., et al.: Realization of the Cirac-Zoller controlled-NOT quantum gate. Nature **422**, 408 (2003)
12. Häffner, H., Hänsel, W., Roos, C.F., et al.: Scalable multiparticle entanglement of trapped ions. Nature **438**, 643 (2005)
13. Matthiesen, C., Yu, Q., Guo, J., et al.: Trapping electrons in a room-temperature microwave Paul trap. Phys. Rev. X **11**, 011019 (2021)
14. Yu, Q., Alonso, A.M., Caminiti, J., et al.: Feasibility study of quantum computing using trapped electrons. Phys. Rev. A **105**, 022420 (2022)
15. Knill, E., Laflamme, R., Milburn, G.J.: A scheme for efficient quantum computation with linear optics. Nature **409**, 46 (2001)
16. Kok, P., Munro, W.J., Nemoto, K., et al.: Linear optical quantum computing with photonic qubits. Rev. Mod. Phys. **79**, 135 (2007)
17. Zajac, D.M., Hazard, T.M., Mi, X., et al.: Scalable gate architecture for a one-dimensional array of semiconductor spin qubits. Phys. Rev. Appl. **6**, 054013 (2016)
18. Jones, C., Fogarty, M.A., Morello, A., et al.: Logical qubit in a linear array of semiconductor quantum dots. Phys. Rev. X **8**, 021058 (2018)
19. Platzman, P.M., Dykman, M.I.: Quantum computing with electrons floating on liquid Helium. Science **284**, 1967 (1999)
20. Lyon, S.A.: Spin-based quantum computing using electrons on liquid helium. Phys. Rev. A **74**, 052338 (2006)
21. Dykman, M.I., Platzman, P.M., Seddighrad, P.: Qubits with electrons on liquid helium. Phys. Rev. B **67**, 155402 (2003)
22. Koolstra, G., Yang, G., Schuster, D.I.: Coupling a single electron on superfluid helium to a superconducting resonator. Nat. Commun. **10**, 5323 (2019)
23. Zhang, M., Jia, H.Y., Wei, L.F.: Jaynes-Cummings models with trapped electrons on liquid helium. Phys. Rev. A **80**, 055801 (2009)
24. Zhang, M., Jia, H.Y., Huang, J.S., et al.: Strong couplings between artificial atoms and terahertz cavities. Opt. Lett. **35**, 1686 (2010)
25. Kawakami, E., Elarabi, A., Konstantinov, D.: Relaxation of the excited rydberg states of surface electrons on liquid Helium. Phys. Rev. Lett. **126**, 106802 (2021)
26. Zou, S., Konstantinov, D.: Image-charge detection of the Rydberg transition of electrons on superfluid helium confined in a microchannel structure. New J. Phys. **24**, 103026 (2022)
27. Schuster, D.I., Fragner, A., Dykman, M.I., et al.: Proposal for manipulating and detecting spin and orbital states of trapped electrons on Helium using cavity quantum electrodynamics. Phys. Rev. Lett. **105**, 040503 (2010)
28. Grimes, C.C., Adams, G.: Evidence for a liquid-to-crystal phase transition in a classical, two-dimensional sheet of electrons. Phys. Rev. Lett. **42**, 795 (1979)
29. Grimes, C.C., Brown, T.R., Burns, M.L., et al.: Spectroscopy of electrons in image-potential-induced surface states outside liquid Helium. Phys. Rev. B **13**, 140 (1976)
30. Woolf, M.A., Rayfield, G.W.: Energy of negative ions in liquid helium by photoelectric injection. Phys. Rev. Lett. **15**, 235 (1965)
31. Grimes, C.C.: Cyclotron resonance in a two-dimensional electron gas on helium surfaces. J. Magn. Magn. Mater. **11**, 32 (1979)
32. Armbrust, N., Güdde, J., Höfer, U.: Spectroscopy and dynamics of a two-dimensional electron gas on ultrathin helium films on Cu(111). Phys. Rev. Lett. **116**, 256801 (2016)
33. Glasson, P., Dotsenko, V., Fozooni, P., et al.: Observation of dynamical ordering in a confined Wigner crystal. Phys. Rev. Lett. **87**, 17 (2001)

34. Fragner, A.A.: Circuit Quantum Electrodynamics with Electrons on Helium. Yale University, PhD Theses (2013)
35. Gao, F., Wang, J.H., Watzinger, H., et al.: Site-controlled uniform Ge/Si hut wires with electrically tunable spin-orbit coupling. Adv. Mater. **32**, 1906523 (2020)
36. Yang, G.: Circuit Quantum Electrodynamics with Electrons on Helium. PhD Thesis, University of Chicago (2020)
37. Blais, A., Grimsmo, A.L., Girvin, S.M., et al.: Circuit quantum electrodynamics. Rev. Mod. Phys. **93**, 025005 (2021)
38. Göppl, M., Fragner, A., Baur, M., et al.: Coplanar waveguide resonators for circuit quantum electrodynamics. J. Appl. Phys. **104**, 113904 (2008)
39. Cridland, A., Lacy, J.H., Pinder, J., et al.: Single microwave photon detection with a trapped electron. Photonics **3**, 59 (2016)
40. Blais, A., Huang, R.S., Wallraff, A., et al.: Cavity quantum electrodynamics for superconducting electrical circuits: an architecture for quantum computation. Phys. Rev. A **69**, 062320 (2004)
41. Blais, A., Gambetta, J., Wallraff, A., et al.: Quantum-information processing with circuit quantum electrodynamics. Phys. Rev. A **75**, 032329 (2007)
42. Raha, M., Chen, S.T., Phenicie, C.M., et al.: Optical quantum nondemolition measurement of a single rare earth ion qubit. Nat. Commun. **11**, 1605 (2020)
43. Gómez-León, Á., Luis, F., Zueco, D.: Dispersive readout of molecular spin qudits. Phys. Rev. Applied **17**, 064030 (2022)
44. Zhou, X.J., Koolstra, G., Zhang, X.F., et al.: Single electrons on solid neon as a solid-state qubit platform. Nature **605**, 46 (2022)
45. You, Z., Chio, C.H., Hoi, I.C., et al.: Phase shifting control for IQ separation in qubit state tomography. Quantum Inf. Process. **23**, 19 (2024)
46. Walls, D.F., Milburn, G.J.: Quantum Optics. Physics Today. Springer-Verlag, Berlin (1995)
47. Jeffrey, E., Sank, D., Mutus, J.Y., et al.: Fast accurate state measurement in superconducting qubits. Phys. Rev. Lett. **112**, 190504 (2014)
48. He, Q., Ouyang, P., Gao, H., He, S., et al.: Low-loss superconducting aluminum microwave coplanar waveguide resonators on sapphires for the qubit readouts. Supercond. Sci. Technol. **35**, 065017 (2022)